AIAA JOURNAL
Vol. 43, No. 3, March 2005

Interaction of Plume with Shock Waves in Laser Ablation

Diomar Cesar Lobao*
Concordia University, Montreal, Quebec H3G 1M8, Canada
and
Alex Povitsky†
University of Akron, Akron, Ohio 44325-3901

This study is focused on numerical modeling of evolution of ablated plume in laser furnace. The temperature of catalyst particles embedded in plume is crucial for the formation of carbon nanotubes from gaseous carbon. The proposed model includes compressible Euler equations combined with a multispecies formulation for concentration of chemical components describing the plume expansion into surrounding gas. To obtain the thermal behavior of catalyst particles the Eulerian solver has been combined with Lagrangian tracking of catalyst particles. The chamber pressure, geometry of the carbon target, plume emerging velocity, and the time interval between injections of the plume dramatically affect the thermal behavior of catalyst particles. The results of modeling have shown that the increase of plume injection velocity raises the temperature of particles but also increases the oscillations of particles temperature. The low chamber pressure helps to avoid temperature oscillations of catalyst particles because the plume moves far behind strong reflected shock waves; however, complex motion of particles at the vicinity of slip lines causes temperature oscillations. Whereas previous studies were focused on the evolution of a single plume, this study shows that the dynamics and thermal regime of multiple plumes are different from those of a single plume.

Nomenclature

C_1, C_2	=	mass concentration (mass fraction) of plume material and furnace gas
$c(x, t)$	=	freezing speed in relaxing total variation diminishing scheme
c_∞	=	speed of sound in undisturbed furnace gas
E	=	total energy per volume unit volume
e	=	internal energy per unit mass
F, G	=	components of flux vector
h	=	total entalpy
J	=	Jacobian
L	=	furnace length
M	=	Mach number
p	=	pressure
R	=	furnace radius
R_1, R_2	=	gas constants of plume material and furnace gas
(r, x)	=	two-dimensional cylindrical coordinates
S	=	source term
T	=	temperature
t	=	time
U, V	=	contravariant velocity components
u, v	=	Cartesian velocity components
W_1, W_2	=	characteristic variables
γ	=	ratio of specific heats, 1.4
ρ	=	density
ς, η	=	generalized curvilinear coordinates
τ	=	temporal mixing length
ν	=	viscosity
Ω	=	injection velocity of plume material

Presented as Paper 2003-3923 at the AIAA 33rd Fluid Dynamics Conference, Orlando, FL, 23–26 June 2003; received 5 August 2003; revision received 27 September 2004; accepted for publication 27 September 2004.

*Postdoctoral Fellow, Department of Mechanical and Industrial Engineering; currently Adjunct Professor, Department of Mechanical Engineering, Centro Universitário de Volta Redonda, Av. Paulo Erlei Alves Abrantes, No. 1325, Três Poços, 27240-000, Volta Redonda-RJ, Brazil.

†Associate Professor, Department of Mechanical Engineering, College of Engineering. Member AIAA.

I. Introduction

In the laser ablation process, the solid carbon substrate is gasified by the energy of a laser beam. The plume, loaded with catalyst particles, expands explosively into the ambient gas of a laser furnace. Because the initial gas pressure in the ablated plume exceeds 100 atm, shock waves are formed in the ambient gas. The high-pressure initial conditions are similar to those of explosions. In turn, the propagation of incident and reflected shock waves affects the plume behind the incident shock wave. The plume mixing with furnace gas is caused by the Raleigh–Taylor instability at the plume-to-gas interface, whereas the reflected shock wave interacts with the plume.

The thermal behavior of metallic submicrometer particles is critical for the synthesis of carbon nanotubes because the formation of nanotubes starts at the surface of catalysts.[1,2] The reasons for the nonmonotonic temperature of catalysts in the developing plume are different from those in a compressible steady turbulent flow. The overall time interval considered ($\sim$200 μs) is comparable to the lifetime of a single turbulent mole. The surrounding inert gas may be turbulent, but it has a relatively small average velocity of $\sim$1 m/s that is much smaller than the velocity of particles in the plume. Therefore, the turbulent diffusion has only a minor influence on temperature oscillations of particles for the considered time interval. On the other hand, the unsteady reflected shock waves and slip lines interact with catalysts and cause strong temperature oscillations.

The widely used experimental facility known as a laser furnace is shown in Ref. 1. Puretzky et al.[2] investigated a single-wall carbon nanotube growth by time-restricted laser vaporization and presented images of Rayleigh-scattered light from the C/Ni/Co plume after laser ablation inside the furnace. Computational results of the concentration of ablated chemical species for a single plume are presented by Greendyke et al.[3] Unfortunately, there are no available experimental or computational results on the temperature of individual catalyst particles. Experimental measurements of the temperature of catalyst particles that fly with supersonic speed in explosive plume expansion are not feasible. Therefore, numerical

modeling is the primary way to obtain the thermal behavior of catalyst particle injected with the plume.

Many issues of the long-term (>100-μs range) behavior of ablated plumes have not been studied in detail in the past, especially those related to plume interaction with reflected shock waves and backward plume motion in the confined space of the laser furnace. Analytical results relevant to the plume dynamics of laser ablation are limited to the point explosion followed by the spherical expansion into the vacuum.[4] The attempts to use these analytical results are limited to the initial phase of the plume development (typically within the first dozen of microseconds after ablation).[5] The furnace chamber confines the plume and produces reflected shock waves that are not accounted for by the analytical model. In experiments, the ambient laser furnace gas pressure varies from near-vacuum to atmospheric pressure.[6,7] The average pressure in the laser furnace determines the speed of propagation of incident and reflected shock waves and the location of the plume with respect to shock waves. The proposed computational model predicts the temperature profile of particles crossing the reflected shock waves.

The known processes of the synthesis of carbon nanotubes include laser ablation (LA), chemical vapor deposition, and decomposition of high-pressure carbon oxide (HiPco). All of these processes are controlled by metal catalyst particles that initiate the synthesis of carbon nanotubes from the feed-stock gas or ejected plume. The HiPco process is based on the synthesis of carbon nanotubes in the carbon oxide atmosphere where turbulent steady subsonic jets mix in a high-pressure reactor. The thermal dynamics of catalyst particles is critical for the formation of carbon nanotubes, as has recently been shown for the HiPco process.[8,9] Similar to the HiPco modeling,[9] the LA model proposed in the current study is based on the combined Eulerian and Lagrangian approach applied to the tracking of the trajectories of catalyst particles.

In the present study, the implemented numerical model has to be accurate and stable in a broad range of gas pressures, ranking from a low ambient pressure of $\approx 10^{-2}$ atm to a very high pressure of $\approx$100 atm behind the blast wave at the initial stage of the plume evolution. In the majority of LA technologies, the laser hits the surface periodically, and the series of plumes emerge as a result of LA of the solid substrate. However, in the available computational fluid dynamics (CFD) literature, only the propagation of a single plume is considered.[3]

The goal of this paper is to obtain the temperature of catalyst particles as a function of time; to show the influence of chamber pressure, injection velocity, and periodicity of the plume on the temperature profile; and to discuss physical reasons for nonmonotonic temperature behavior of catalyst particles. This temperature as a function of time is needed to model chemical reactions leading to the nucleation of nanotubes. One of objectives of this study is to examine the influence of a multiple (periodic in time) plume injection on the plume dynamics and to investigate the thermal behavior of the catalyst particles in this case.

The concentration of catalyst particles is low, and so the gasdynamics of the plume is not affected by the motion of catalysts, the thermal effect of solidification of catalyst particles, or the thermal effect of nucleation reactions. The temperature dynamics of catalyst particles for the LA process is presented in the current paper, whereas the chemical nucleation model will be addressed in a separate paper. Such a decomposition of a chemical model of nucleation of nanotubes and the CFD-based model of temperature of catalyst particles has been performed in our recent HiPco modeling.[8]

This paper contains the following sections: In Sec. II, a mathematical model of plume dynamics is introduced and validity of the inviscid assumption in plume dynamics is discussed. In Sec. III, the adopted relaxing total variation diminishing (TVD) numerical scheme is briefly described and the implementation of this scheme to the benchmark one-dimensional and two-dimensional cases pertinent to plume modeling and the accuracy of the scheme are discussed. The Lagrangian approach to tracking the position and temperature of the catalyst particles is also described in Sec. III. In Sec. IV, the obtained single-plume dynamics is presented for near-vacuum and atmospheric pressure of the furnace gas and for the broad range of plume injection velocities. In Sec. V, a multiple-plume dynamics emerging from a periodic laser hit is discussed.

II. Mathematical Model

The model of plume evolution is based on compressible unsteady multispecies Euler equations. The short duration of investigated phenomena calls for the inviscid model of plume mixing. The effective viscous length scale is defined by $l_{\text{visc}} = \sqrt{(\nu\tau)}$, where ν is effective viscosity and τ is the timescale of modeled phenomena. This method of evaluating the influence of viscous forces has been used by Quirk and Karni[10] and in numerous other studies dealing with the shock wave interaction with flow inhomogeneities.[11]

For the considered range of the chemical composition of the gas–plume mixture, the temperatures, and the time interval of 200 μs, the viscous length scale is $l_{\text{visc}} \sim 100\ \mu$. This scale is two orders of magnitude smaller than the cross section of the plume. Nevertheless, the viscous force is dominant for the dynamics of submicrometer catalyst particles. (See the discussion in Sec. III about the Lagrangian approach to model the motion of catalyst particles.) For multiple-plume injection, the effect of viscous stresses and turbulence on plume development will be investigated in separate research.

Although cylindrical geometry of the computational domain is used in the presented simulations, generalized coordinates ξ and η are needed to study the focusing of shock waves on the plume or the suppression of shock waves by the use of more complex geometry:

$$\frac{\partial \boldsymbol{Q}}{\partial t} + \frac{\partial \boldsymbol{F}}{\partial \xi} + \frac{\partial \boldsymbol{G}}{\partial \eta} = \boldsymbol{S} \tag{1}$$

where the vectors of conserved variables and fluxes are given by

$$\boldsymbol{Q} = \frac{\delta}{J}\begin{bmatrix} \rho \\ \rho u \\ \rho v \\ E \\ \rho C_1 \\ \rho C_2 \end{bmatrix}, \qquad \boldsymbol{F} = \frac{\delta}{J}\begin{bmatrix} \rho U \\ \rho u U + \xi_x p \\ \rho v U + \xi_y p \\ (E+p)U \\ \rho C_1 U \\ \rho C_2 U \end{bmatrix}$$

$$\boldsymbol{G} = \frac{\delta}{J}\begin{bmatrix} \rho V \\ \rho v V + \eta_x p \\ \rho v V + \eta_y p \\ (E+p)V \\ \rho C_1 V \\ \rho C_2 V \end{bmatrix}, \qquad \boldsymbol{S} = \frac{1}{J}\begin{bmatrix} 0 \\ 0 \\ p \\ 0 \\ 0 \\ 0 \end{bmatrix} \tag{2}$$

where U and V are the contravariant velocities[12] in the directions normal to constant ξ and η surfaces, respectively, and C_1 and C_2 are the mass fractions of the plume material (carbon C3) and furnace gas (argon), respectively. The implemented numerical method can be easily extended to an arbitrary number of species. The Jacobian of a coordinate transformation is given by $J = 1/(x_\xi y_\eta - x_\eta y_\xi)$. In the numerical scheme used, the metrics of coordinate transformation are approximated by second-order finite differences. Second-order three-point backward finite differences are used for the boundary points. For the two-dimensional Cartesian coordinates $\delta = 0$, whereas for the cylindrical two-dimensional (x, r) coordinates $\delta = \eta$. For generality, all variables are nondimensionalized by the use of freestream quantities corresponding to the undisturbed furnace gas at furnace temperature and pressure. The total energy is defined by $E = -p + \rho(u^2 + v^2)/2 + \rho h$, where h is the enthalpy per unit mass for each species.

The equation of state for multispecies flow can be written as

$$p = \sum_{i=1}^{2} p_i = \sum_{i=1}^{2} \rho C_i R_i T = \rho\left(\sum_{i=1}^{2} C_i R_i\right) T = \rho R T \tag{3}$$

where gas constant R is defined as

$$R = \sum_{i=1}^{i=2} C_i R_i$$

In the present research, the calorically perfect gas model is adopted. The calorically perfect gas assumption overestimates the gas temperature, and the refinement of the gas thermal model will be addressed in future research.

III. Numerical Methodology

To discretize the Euler equations (1), the second-order upwind numerical scheme for conservation laws (MUSCL), together with the relaxing TVD scheme, are used in the current study. Relaxation methods make use of the characteristic variables of the system and the finite speed of wave propagation and do not need Riemann solvers. (See Sec. III.A for details.) The relaxing TVD scheme is similar to central schemes described in Refs. 13 and 14. In two-dimensional cases, system (1) can be split with the Strang technique[15] into two separate one-dimensional equations that are solved in a sequential way. The relaxing TVD scheme offers easier implementation than a conventional TVD scheme because there is no need to calculate the flux Jacobian eigenvectors matrices for the Euler equations. This makes the numerical algorithm particularly efficient for multispecies problems and/or reactive chemical systems. More details about the numerical methodology and its application to curvilinear laser furnaces are available in Ref. 16.

A. Relaxing TVD Scheme

The solution of a one-dimensional system of conservation laws is described by the use of the relaxing TVD scheme:

$$\frac{\partial q}{\partial t} + \frac{\partial \boldsymbol{F}(q)}{\partial x} = 0 \tag{4}$$

This system is replaced by the relaxing system as

$$\frac{\partial q}{\partial t} + \frac{\partial cv}{\partial x} = 0, \qquad \frac{\partial v}{\partial t} + \frac{\partial cq}{\partial x} = 0 \tag{5}$$

where $v = \boldsymbol{F}(q)/c$ and $c(x, t)$ is a free parameter called the freezing speed.[17] This system is also called the relaxation system and is used to calculate fluxes, whereas explicit time integration is implemented by the use of a second-order Runge–Kutta method. It is shown that this scheme is TVD[17] under the constraint that c is greater than the characteristic speed $u = \partial \boldsymbol{F}/\partial q$. One way to satisfy this condition is to define $c = |u| + a$, where a is the local speed of sound.

To solve the relaxed system, it is decoupled with characteristic variables $W_1 = (q + v)/2$ and $W_2 = (q - v)/2$. The obtained linear system of equations with respect to unknown W_1 and W_2 has been discretized in space with the MUSCL scheme as described in Ref. 18.

To validate the accuracy of the aforementioned numerical discretization, the second-order differences (Sod's) shock-tube one-dimensional test case was carried out by the use of the relaxing TVD and the upwind TVD schemes for comparison (see Refs. 19 and 20). The numerical results and the analytical solution at $t = 0.1644$ are shown in Figs. 1a and 1b, respectively. The solution includes a left rarefraction wave, contact discontinuity, and right shock wave. The initial conditions are $(\rho, u, p) = (1.0, 0, 2.5)$ if $0 \le x < 0.5$ and (0.125, 0, 0.25) if $0.5 \le x \le 1.0$. In numerical computations, the Courant–Friedrichs–Lewy (CFL) number is equal to 0.75, and the number of numerical grid points is assumed equal to 500.

As can be seen in Figs. 1a and 1b, the shock wave and contact discontinuity are captured in their expected positions by both schemes. The shock is captured over two numerical grid cells for the upwind TVD scheme and over one cell for the relaxing TVD scheme. For the upwind TVD solution, the discontinuity is smeared as compared to the relaxing TVD solution. These results demonstrate the better resolution quality of the relaxing TVD scheme than that of the upwind TVD scheme.

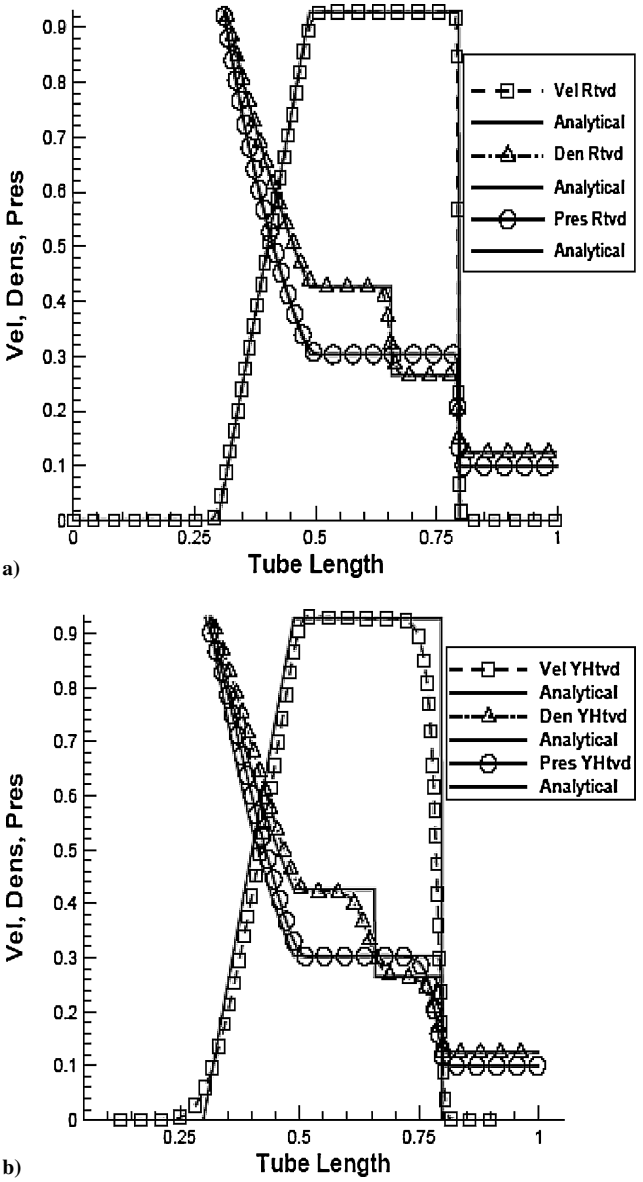

Fig. 1 One-dimensional Sod shock tube, distribution of velocity (Vel), density (Den), and pressure (Pres): a) relaxing TVD scheme (Rtvd) and b) Yee–Harten TVD scheme (YHtvd).

A validation test for Sod's two-dimensional problem is carried out with the relaxing TVD scheme in both spatial directions. For two-dimensional problems, the Strang splitting technique[15] is applied to the two-dimensional extension of system (5). By the use of dimensional splitting, it is a straightforward task to implement the code in a vector processing environment. The initial conditions are prescribed in a square domain $[2,2] \times [2,2]$ to simulate the breakdown of a thin quadrant diaphragm centered at the square center.[21]

The initial conditions are set up as 1.0, 0.0, 0.0, and 2.5 if (x, y) is in the second or fourth quadrant and 0.1, 0.0, 0.0, and 0.25 otherwise.

The 100×100 numerical mesh is used, the time of integration $t = 0.16$, and the CFL number is assumed equal to 0.25. In Fig. 2, density contours are shown with 15 uniformly distributed levels. Computational results are in very good agreement with those presented in Refs. 22 and 23.

B. Lagrangian Approach to Computation of Motion and Temperature of Catalyst Particles

The 10 uniformly distributed initial positions for the catalyst particles are chosen at the laser spot. The catalysts are metallic (Ni) submicrometer particles that are assumed to be ejected and to move with the speed of the plume. The particles are numbered from 1 to 10,

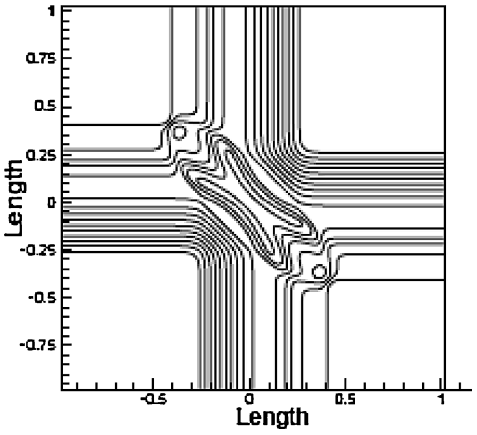

Fig. 2 Two-dimensional Sod problem solved with relaxing TVD scheme, isolines of density.

where the first particle emerges from the point near the center of the laser target and the 10th particle emerges from the periphery of the target. Particles were selected in such a way that their starting points are uniformly distributed across the ablated target. Their injection velocity and initial temperature are equal to those of the plume. For the chemical composition and temperature of the plume and furnace gas mixture over the considered time interval of 200 μs, the viscous length scale $l_{\text{visc}} \sim 100\ \mu$. The catalyst particles are ejected with the plume in the form of either atomic/molecular vapor or liquid clusters of molecules. In general, the atoms/molecules can diffuse in the surrounding gas and deviate from streamlines. Nevertheless, the length scale of diffusion in gas is of the same order of magnitude as the viscous length scale of momentum transfer. Thus, it is assumed that the submicrometer catalysts follow the path lines of the gaseous plume and that the particles' temperature is equal to the local gas temperature.

The viscous length scale is two orders of magnitude larger than the diameter of the catalyst particles. Therefore, the viscous drag force is the major force acting on a catalyst particle. Recall that the influence of viscous forces on plume mixing can be neglected as described earlier in this section. For high-speed plume motion, the Brownian motion of particles and the thermophoresis phenomena can be neglected.[9] The particles' rotation is neglected. Because of the small concentration of particles, the particles do not interact with each other. The latent heat of solidification of catalysts and thermal radiation are neglected, and the temperature of the particles is assumed equal to the local plume temperature. In general, the presence of exothermal and endothermic reactions of the nucleation of nanotubes might change the temperature of catalyst particles. This will be accounted for in a separate study on the chemical kinetics of nucleation of nanotubes.

A Runge–Kutta second-order explicit scheme is used to obtain particles' positions and velocities as functions of time. The Lagrange approach has an advantage over the Euler approach because it gives the temperature of each catalyst particle as a function of time explicitly. Having the temperature of catalyst particles as a function of time will make it possible to model the kinetics of the formation of carbon nanotubes in the same way it was for the HiPco process.[8]

C. Initial and Boundary Conditions

The computational setup follows the description of the experimental facility[2,3] where the radiation of a laser beam is focused on the carbon solid target. The diameter of the focusing spot is 5 mm, and the target is placed inside a chamber containing argon at 1 atm and 1500 K. The duration of a single plume injection is assumed to be equal to 20 ns. The laser fluence is equal to 1.5 J/cm^2. Greendyke et al.[3] computed the boundary pressure and temperature at the laser spot with the Clausius–Clapeyron equation. The Clausius–Clapeyron equation assumes a low density of vapor compared to a solid and uses the ideal gas equation for vapor. Under these conditions, the laser delivers energy that ablates the gaseous

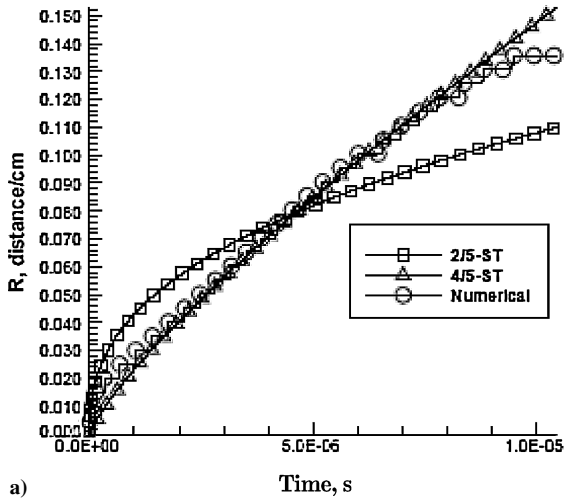

a)

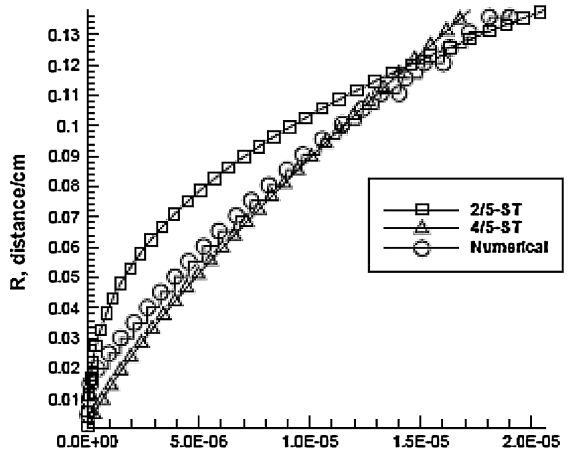

b)

Fig. 3 Dynamics of incident shock wave at earlier stage of LA: position of the front R as a function of time t: a) low surrounding pressure of 0.01 atm and b) atmospheric surrounding pressure of 1.0 atm.

dense plume at 100 atm and 5000 K. This temperature of the solid target corresponds to experimental measurements.[2] In the current study, the plume is assumed to contain C3 carbon that obeys the ideal gas law. The cylindrical furnace chamber has a diameter of 5.0 cm and a length of 25 cm.

The physical domain is discretized in a computational domain by the use of a uniform grid with 200×50 nodes in the axial and radial directions, respectively. Computational results are presented in normalized coordinates $(x/L, r/L)$, where x is the axial symmetrical coordinate, r is the radial coordinate, and L is the length of the laser furnace. For the considered laser furnace, the radial coordinate varies from 0 to 0.1: $0 \le r/L \le R/L = 0.1$. The initial conditions of pressure, temperature, and injection velocity of the emerging plume at the grid points corresponding to the laser target were maintained during the plume emergence. At the end of this time period, the injection velocity is zeroed at the target boundary and replaced by the boundary conditions of a solid adiabatic wall.

The outflow boundary condition is set as an adjustable sub/supersonic boundary. The no-slip and nonpenetrating velocity boundary conditions are imposed at the solid walls of the laser furnace. At the axis of symmetry ($r = 0$), a simple extrapolation boundary condition is adopted.

In all simulations, a sequence of CFL numbers was used to integrate the equations with the maximum possible time step and to avoid the blowup of the solution due to the large pressure gradients, which could cause nonlinear instability. For the first 180 time steps, the CFL of 0.0001 was used; therefore, the time step is of the order of 10^{-11} s at the beginning of time integration. To proceed with the

time integration, the series of increasing CFL numbers 0.001, 0.01, 0.1, 0.3, and 0.5 was used where the CFL number increased after each 180 time steps.

IV. Results of Modeling of Evolution of Single Plume

The Sedov–Taylor two-dimensional blast shock wave problem has been used in our preliminary research[16] as a test case of point explosion where a large amount of energy is liberated in a small volume and the blast wave propagates in the vacuum. The confined computational domain of the laser furnace is different from the infinite domain of the Sedov–Taylor blast wave (see Refs. 24 and 25). Nevertheless, the simulation results could be compared against the Sedov–Taylor (S–T) solution at an earlier stage of the blast wave development, until the blast wave hits the side wall of the laser furnace. For zero plume injection velocity and low and high argon ambient pressures of 10^{-2} and 1.0 atm, see Figs. 3a and 3b, respectively.

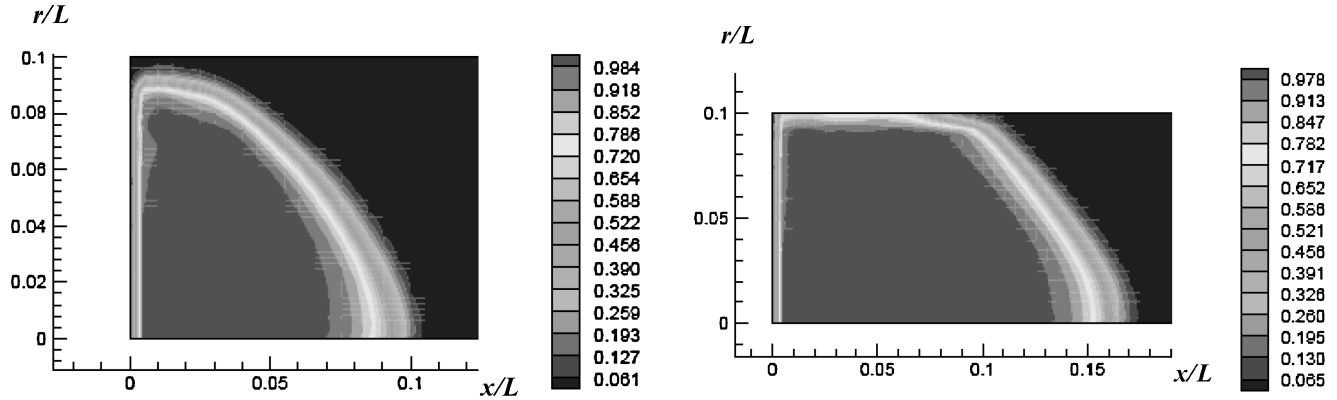

a) b)

Fig. 4 Plume expansion into low ambient pressure, concentration (mass fraction) of carbon C3; computational results in normalized coordinates (x/L, r/L): a) $t = 5.2$ μs and b) $t = 10.0$ μs.

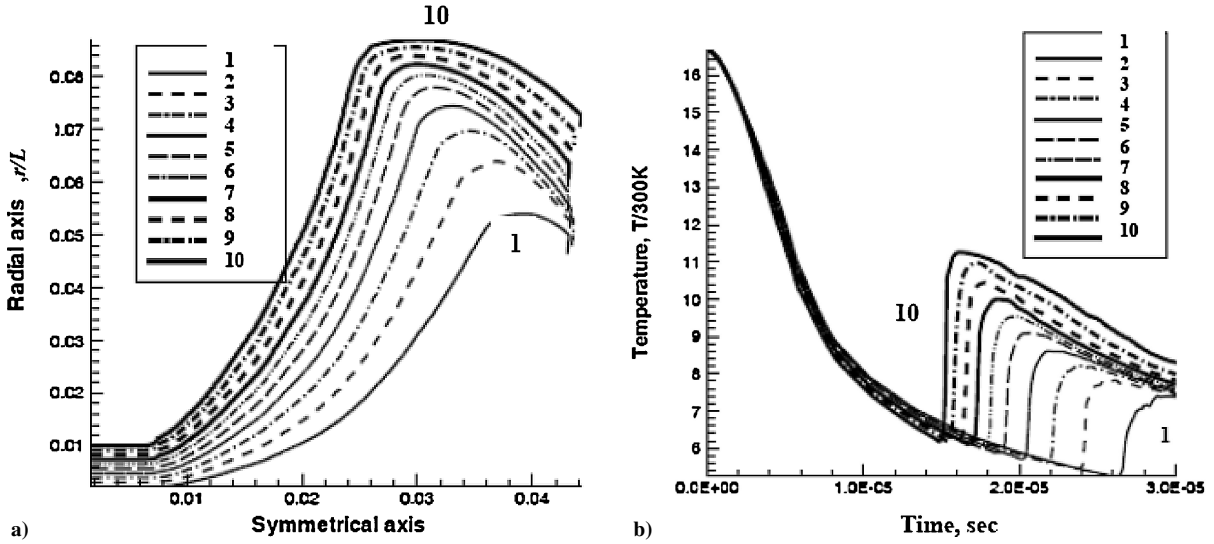

a) b)

Fig. 5 Thermal regime of catalyst particles ejected into low ambient pressure: a) trajectories of injected catalyst particles in spatial coordinates (x/L, r/L) and b) temperature of catalyst particles as function of time.

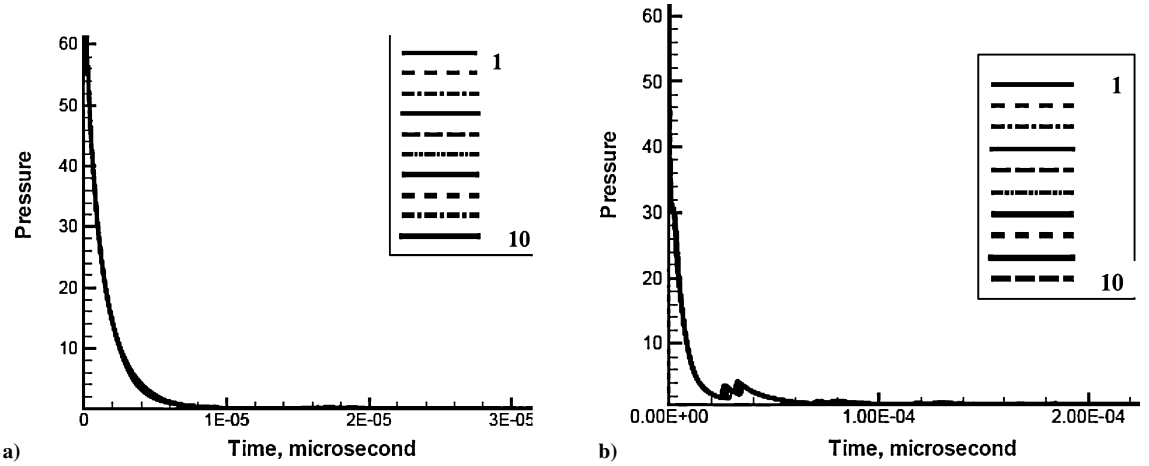

a) b)

Fig. 6 Pressure (atmospheres) along path lines: a) low chamber pressure and b) atmospheric chamber pressure.

As discussed in Ref. 26, the blast wave radius R as a function of time scales with $R \sim t^{(2+\beta)/5}$, where β is a parameter related to the rate of energy deposition. The instantaneous energy deposition corresponds to $\beta = 0$, which is the S–T spherical blast wave solution $R \sim t^{2/5}$. According to Kim et al.[27] the best fit for a laser plasma jet is $\beta = 3$. In the present case, the best fit is obtained for $\beta = 2$ (see Figs. 3a and 3b).

In the theoretical model,[28] $\beta = 2$ is used to account for the continuous energy deposition. A set of simulations with the decreasing plume emergence time from 10.0 to 0.5 ns was performed; the best fitting parameter remains $\beta = 2$ for all considered plume emergence times. According to these numerical experiments, the position of the blast wave front fits the relation $R \sim t^{4/5}$ up to the very short-time energy release of 0.5 ns. The S–T solution with an appropriate value of β fits the numerical wave front speed for low and standard atmospheric pressures because the initial plume-to-ambient gas pressure ratio is relatively large in both cases (10^4 and 10^2, respectively). The limits of the application of the S–T solution are related to plume interaction with side walls, nonzero injection velocity, and multiple-plume injection.

A. Low Chamber Pressure

The material science community expresses strong interest in carrying out LA-based synthesis of nanotubes with very low chamber

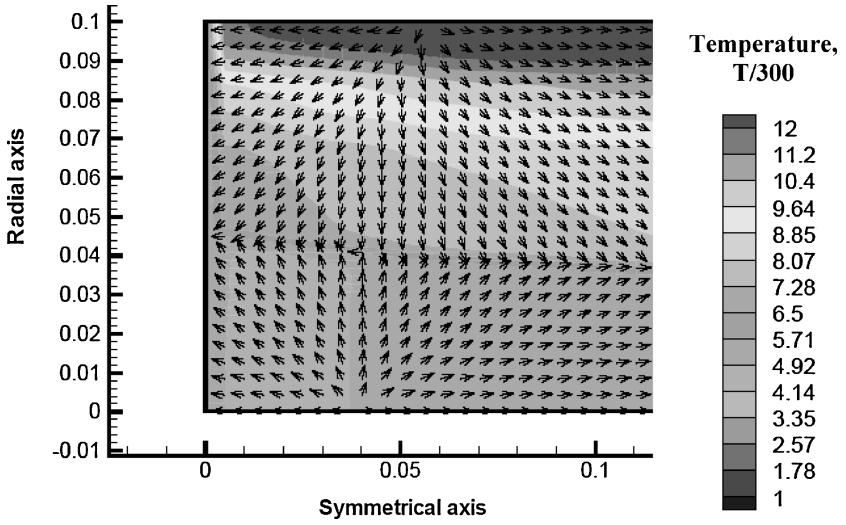

Fig. 7 Slip line in low-pressure chamber at $t = 30$ μs with temperature contours.

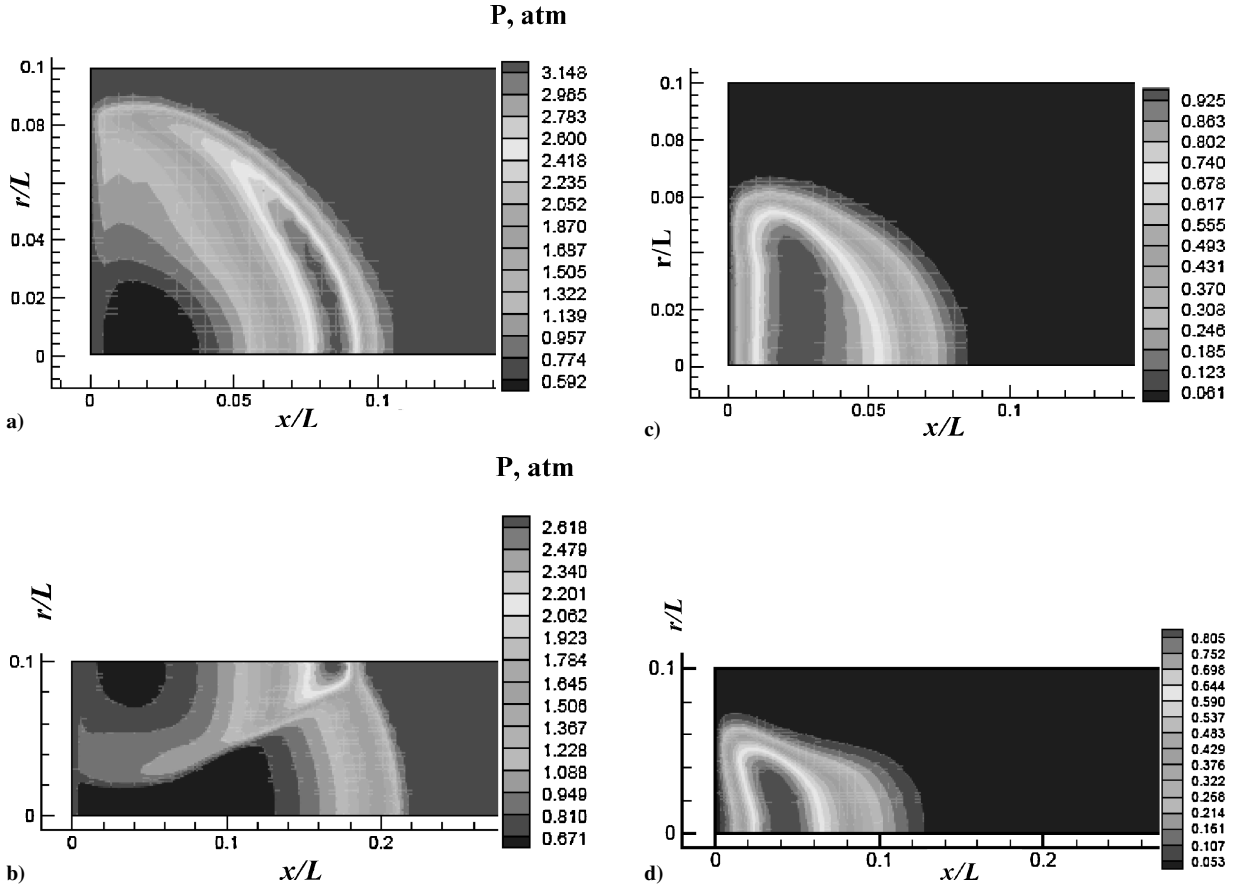

Fig. 8 Shock wave propagation and plume evolution for the standard atmospheric pressure in the laser furnace: a) pressure counters, atmospheres, $t = 10$ μs; b) pressure contours, atmospheres, $t = 37$ μs; c) concentration (mass fraction) of carbon C3, $t = 10$ μs; and d) concentration (mass fraction) of carbon C3, $t = 37$ μs.

gas pressure[6] because the higher ambient gas pressure may halt the production of carbon nanotubes. As the furnace gas pressure decreases to near-vacuum conditions, the plume expansion tends to process at a much higher rate than that for the standard ambient pressure conditions. On the other hand, the near-vacuum conditions are the most challenging for the considered numerical model. The advantage of the relaxing TVD scheme is that the scheme is stable and oscillation free under these conditions, whereas many other numerical schemes show strong instabilities and fail to predict the flowfield if the ambient pressure is close to the vacuum.

The computational results in Fig. 4 are obtained when the ambient pressure of argon is 0.01 atm. The concentration of plume material is shown in Fig. 4a at 5.2 μs. Recall that at this time moment the plume has not yet hit the wall. At a later time moment (Fig. 4b), the plume reaches the wall of the chamber tube, and its shape substantially deviates from the original semispherical surface.

The temperature along path lines corresponding to the aforementioned 10 particles is shown in Fig. 5b for the time interval of 30 μs from the beginning of plume injection. The smooth temperature drop is clearly observed for the initial phase of plume expansion into the vacuum. In Fig. 5a, the trajectories of catalyst particles (path lines) are shown in spatial coordinates $(x/L, r/L)$ to illustrate the complex motion of catalyst particles, where the radial coordinate of particles, that is, the distance from the centerline, appears to be strongly nonmonotonic. This affects the temperature history of catalyst particles as follows. On one side, the pressure along the path lines of catalyst particles is smooth (Fig. 6a). For low ambient pressure, the front blast wave and primary reflected waves are propagated far ahead of the plume. The plume interacts with weak reflected waves that do not cause visible pressure and temperature jumps. On the other side, the unsteady slip lines with strong temperature gradients are still present (Fig. 7) and cause substantial temperature gradients along the path lines of the catalyst particles (Fig. 5b). Numerical experiments have shown that the pressure distribution along path lines is smooth (Fig. 6a). Reflected shock waves are relatively weak when they interact with the plume and do not cause visible temperature oscillations along the trajectories of catalyst particles.

Although the low chamber pressure helps to avoid temperature oscillations of catalyst particles, the complex motion of particles far behind the incident and reflected pressure waves may cause temperature oscillations at a later time. Ejected near the center of the target, the particle, labeled 1, moves in the axial direction for a longer time than other particles. Therefore, its temperature remains monotonic for a longer period of time compared to other particles. The peripheral particles become involved in radial motion at a relatively early stage. (Compare the first and the tenth path lines in Fig. 5a.) Particles move in the radial direction apart from the centerline and pass through regions of higher temperature. In the case of low ambient pressure, the major reason for particles' temperature jumps is the radial motion of particles that reach the vicinity of the slip lines.

B. Atmospheric Chamber Pressure

In most of experiments recorded in literature,[2] the chamber pressure is close to standard atmospheric pressure. The pressure contours are shown in Figs. 8a and 8b for the plume emerging in the laser furnace under the standard pressure at two characteristic time moments, 10 and 37 μs. Computations were conducted at the standard surrounding pressure of 1.0 atm to show how the blast wave propagates and interacts with the tube walls, which in turn, causes interactions of reflected shock waves with the plume.

At 10 μs, a spherical shock wave front is seen moving outward of the laser target. Then, at 37 μs, the expanding bow shock front hits the side solid wall and reflects back. The reflected shock wave recompresses the carbon plume (Fig. 8d) and squeezes the plume, causing the plume temperature to increase up to its maximum at approximately 50 μs (Fig. 9b).

The concentration of plume material is shown in Figs. 8c and 8d at the same time moments as the aforementioned pressure contours (10 and 37 μs, respectively). Although in this case the carbon plume expands at a slower rate than that for the vacuum condition, the speed

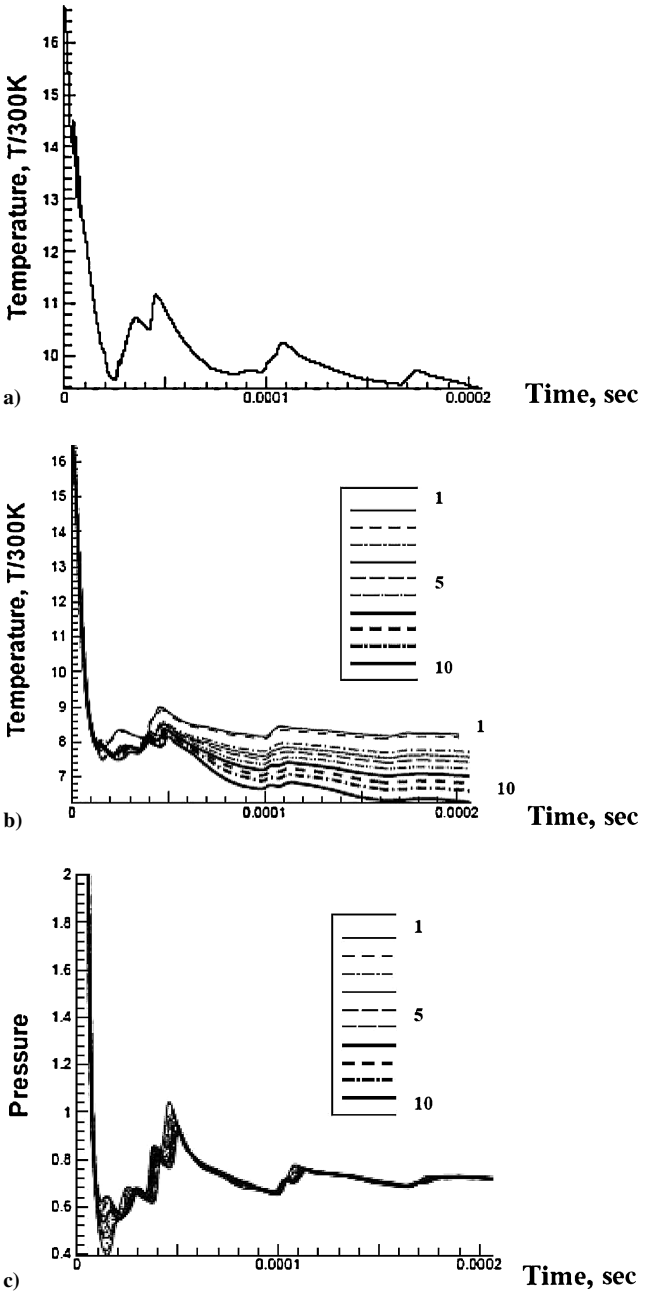

Fig. 9 Peak temperature and temperature of catalyst particles for the standard atmospheric pressure of the surrounding furnace gas: a) peak (maximum spatial) temperature, b) temperature of catalyst particles, and c) pressure (atmospheres) along path lines.

of the incident blast wave propagation is much slower than that for the blast wave propagation into vacuum. Because the plume stays closer to the shock wave, plume interaction with reflected shock waves is more prominent than that for the near-vacuum furnace pressure.

For the time interval of 200 μs, the peak temperature is shown in Fig. 9a, and temperatures of catalyst particles are shown in Fig. 9b as functions of time. The instantaneous peak temperature is the maximum gas temperature in laser furnace at a given time.

In Fig. 9c, the pressure peaks along the trajectories of the catalyst particles are shown. These peaks are caused by the reflected shock wave that first interacts with the plume at the time moment 37 μs. Subsequent interaction of particles with reflected shock waves causes the temperature of catalyst particles to reach a maximum at about 50 μs. This corresponds to the peak furnace temperature achieved at about the same time.

C. Effect of Injection Velocity

In the preceding sections, the plume injection velocity has been assumed equal to zero in all simulations, and so the plume only propagated due to the high initial pressure. In general, plume injection velocity is equal to the rate of carbon mass ablation as it is injected into the flowfield by the laser firing process. To find plume injection velocity and its distribution in space and time, one should model laser-induced melting and vaporization. This is beyond the scope of this paper. In the current research, the feasible range of carbon injection velocities is considered. The features of the temperature dynamics of catalyst particles as a function of injection velocity are discussed in this section.

The gaseous carbon (plume) is released with a velocity, $\Omega = K c_\infty$, where c_∞ is the speed of sound in the undisturbed furnace gas at the average furnace temperature and pressure. The injection velocity $\Omega = 15.0 c_\infty$ was calculated from experiments[2] and used in simulations[3] as an input datum. For $\Omega = 15.0 c_\infty$, the carbon C3 plume concentration is shown in Fig. 10a, and the peak temperature profile as a function of time is shown in Fig. 10b.

To show the influence of vortical regions on trajectories of particles and, in turn, on temperature oscillations, the highly nonmonotonic path lines are shown in Fig. 10c for $t \le 243$ μs. The complex vortical motion of the particles observed in Fig. 10c is caused by the formation of the moving recirculation zone that drives the particles back toward the laser target and forms the mushroom-type shape of the carbon plume (Fig. 10a). At the initial stage, catalyst particles with the initial velocity $\Omega = 15.0 c_\infty$ move straight up to $x/L \approx 0.09$, where they start to spread in a radial direction. For zero injection velocity, the transition to spherical expansion occurs earlier and corresponds to $x/L \approx 0.01$. (Compare Figs. 5a and 10c.) This shows limits of applicability of spherical explosion model to LA for a higher injection speed.

The temperature of catalyst particles substantially increases with the increase of injection velocity. (Compare Figs. 10d and 7b.) The temperature of all considered catalyst particles are close to each other. For larger a injection velocity, the carbon plume propagates faster and is affected more by reflected shock waves. On the other hand, the amplitude of temperature oscillations increases as well, which may cause problems with the performance of particles as good catalysts.

V. Modeling Results for Multiple Plume Ejection

In this section, we consider the dynamics of a series of sequential plumes, in particular the double plume. The description of the

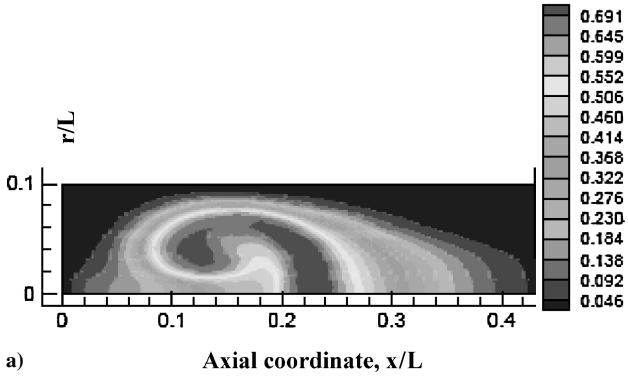

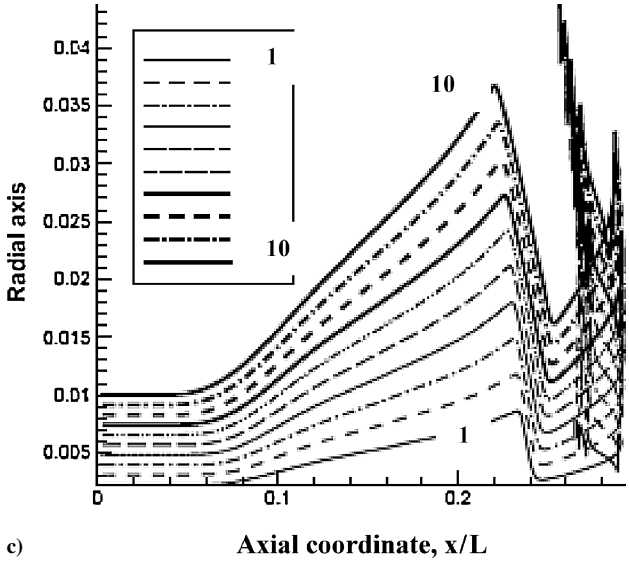

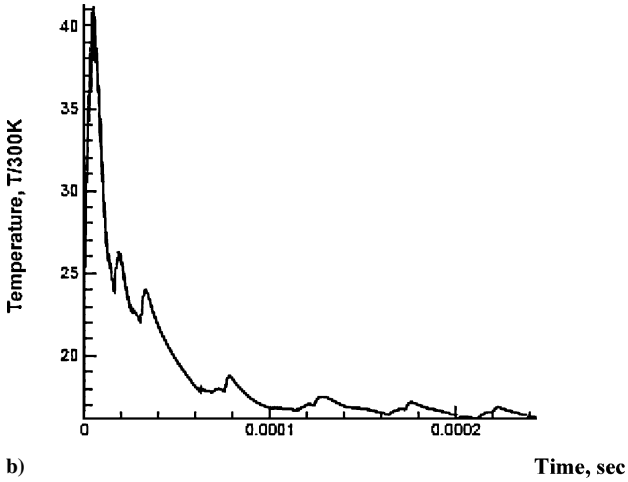

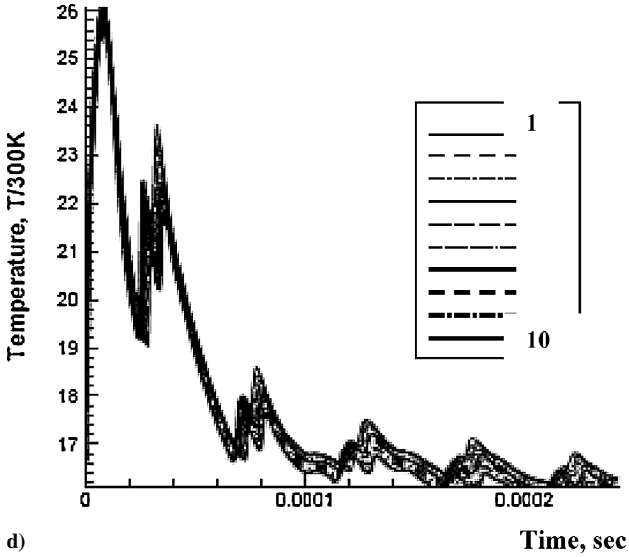

Fig. 10 Plume dynamics and temperature of catalyst particles for injection speed $\Omega = 15.0 c_\infty$: a) mass concentration of carbon C3 at $t = 243$ μs, b) peak temperature, c) trajectories of catalyst particles, and d) temperature of catalyst particles ($t \le 243$ μs).

dynamics of double plume represents the first departure from a single-plume model toward a series of ejected plumes. The effect of plume multiplicity on the ablation process are important for surface modification of materials[29] and matrix-assisted laser desorption ionization.[30] The pressure and velocity field, created by the first plume, significantly affect the dynamics of the second plume. The temperature dynamics of catalyst particles ejected with plumes appears to be different for the first and the second plumes and different from that for a single-plume model. In the current study, the initial pressure and temperature of injected plumes are assumed to be the same for the first and the second plume. In general, part of the laser energy is absorbed by the plume ahead of the current plume, and the deposited energy at the target will not be the same for the two plumes.[5] This issue will be addressed in future research.

In the current study, the second plume is irradiated 16.0 μs after the first plume has emerged. The first series of results shown in Fig. 11 has been obtained for zero injection velocity and standard atmospheric pressure of the laser furnace. Figure 11a shows pressure

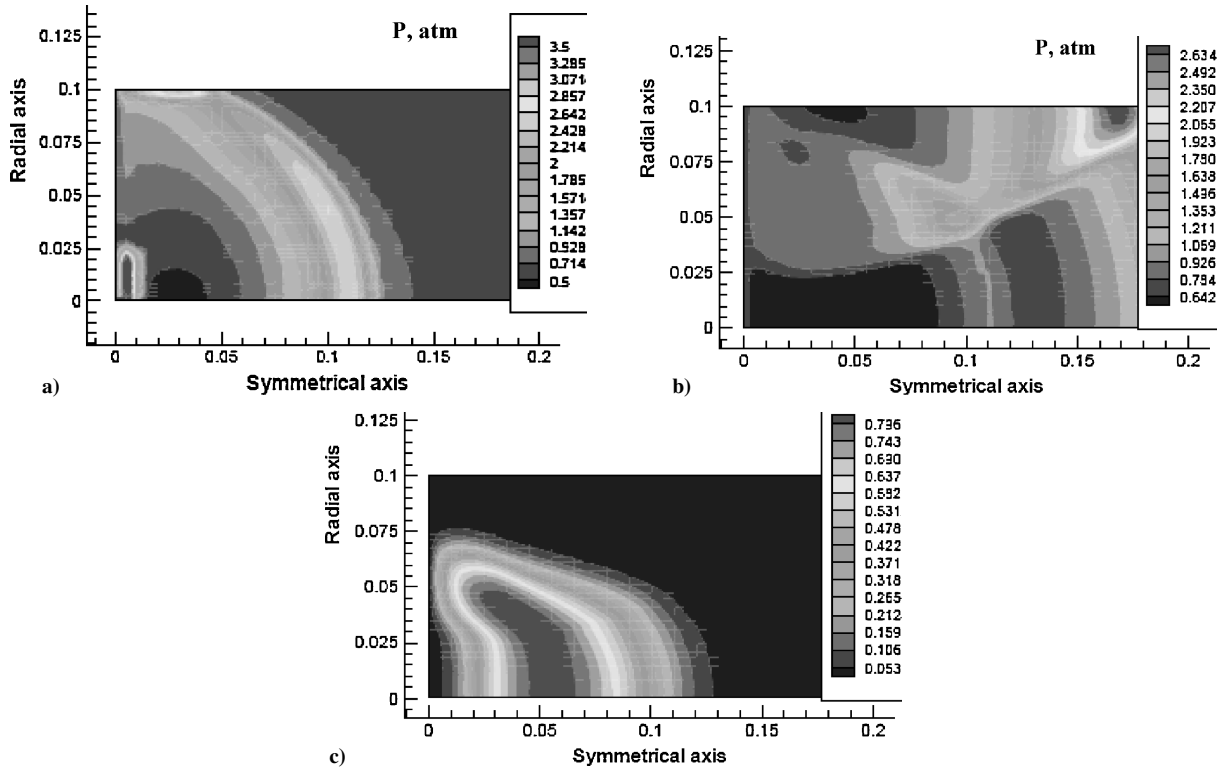

Fig. 11 Plume dynamics for doubled plume emerging with zero injection velocity; normalized coordinates (x/L, r/L): a) pressure contours (atmospheres) at $t = 16.0$ μs when the second plume emerges, b) pressure contours at $t = 34.0$ μs, and c) concentration (mass fraction) of carbon C3 at $t = 34.0$ μs.

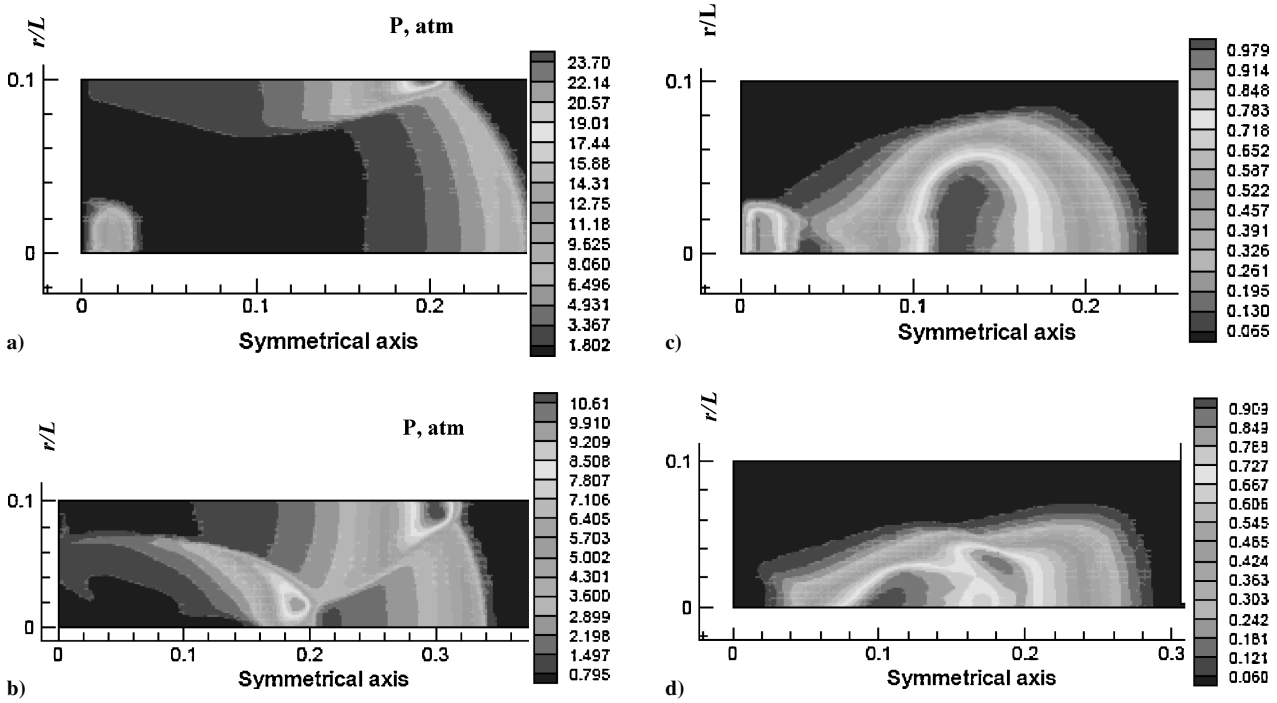

Fig. 12 Plume dynamics for doubled plume with injection velocity $\Omega = 15c_\infty$: a) pressure contours (atmospheres), $t = 16$ μs; b) pressure contours (atmospheres), $t = 26$ μs; c) contours of concentration (mass fraction) at time $t = 16$ μs; and d) contours of concentration (mass fraction) at time $t = 26$ μs.

contours immediately after the second pulse has been irradiated at 16.0 μs. In Figs. 11b and 11c, the pressure contours and the concentration of carbon are shown at 34.0 μs, that is, 18.0 μs after the second pulse has emerged. At this stage, the two plumes merge completely. Figure 11b shows the shock wave generated by the second pulse on its way to interact with the first shock wave at the time moment $t = 34.0$ μs. The interaction of the reflected waves corresponding to the first and to the second plume is clearly seen in Fig. 11b.

Plume injection velocity Ω has a strong influence on the interaction between two plumes. The plumes injection velocity is equal to $15c_\infty$ for numerical results shown in Fig. 10. Pressure and concentration of plume material are shown in Figs. 12a and 12c immediately after the second pulse has emerged at 16.0 μs. In Figs. 12b and 12d, the concentration of plume material and pressure are shown at 26.0 μs. The interaction between the second and first plumes creates a complex nonmonotonic concentration field, $C_1(x, r)$, of plume material. Figure 12b shows the interaction of an incident blast wave created by the second plume with the reflected shock waves produced by the blast wave associated with the first plume. The trajectories and temperature of catalyst particles are shown separately in Fig. 13 for particles that emerged with the first plume and with the second plume.

The trajectories of catalyst particles emerging with the first plume, as well as their temperature dynamics, are shown in Figs. 13a and 13b, respectively, for $t = 243$ μs. Trajectories of catalyst particles corresponding to the first plume turn back according to the mushroom-type shape of the plume, which is shown in Fig. 13e at 243 μs.

The temperature of catalyst particles for the first plume appears to be somewhat similar to that for the single plume (Fig. 10b). However, the peak at $\approx$30 μs has increased by approximately 1650 K (cf. Figs. 13b and 10b) due to interactions of reflected shock waves

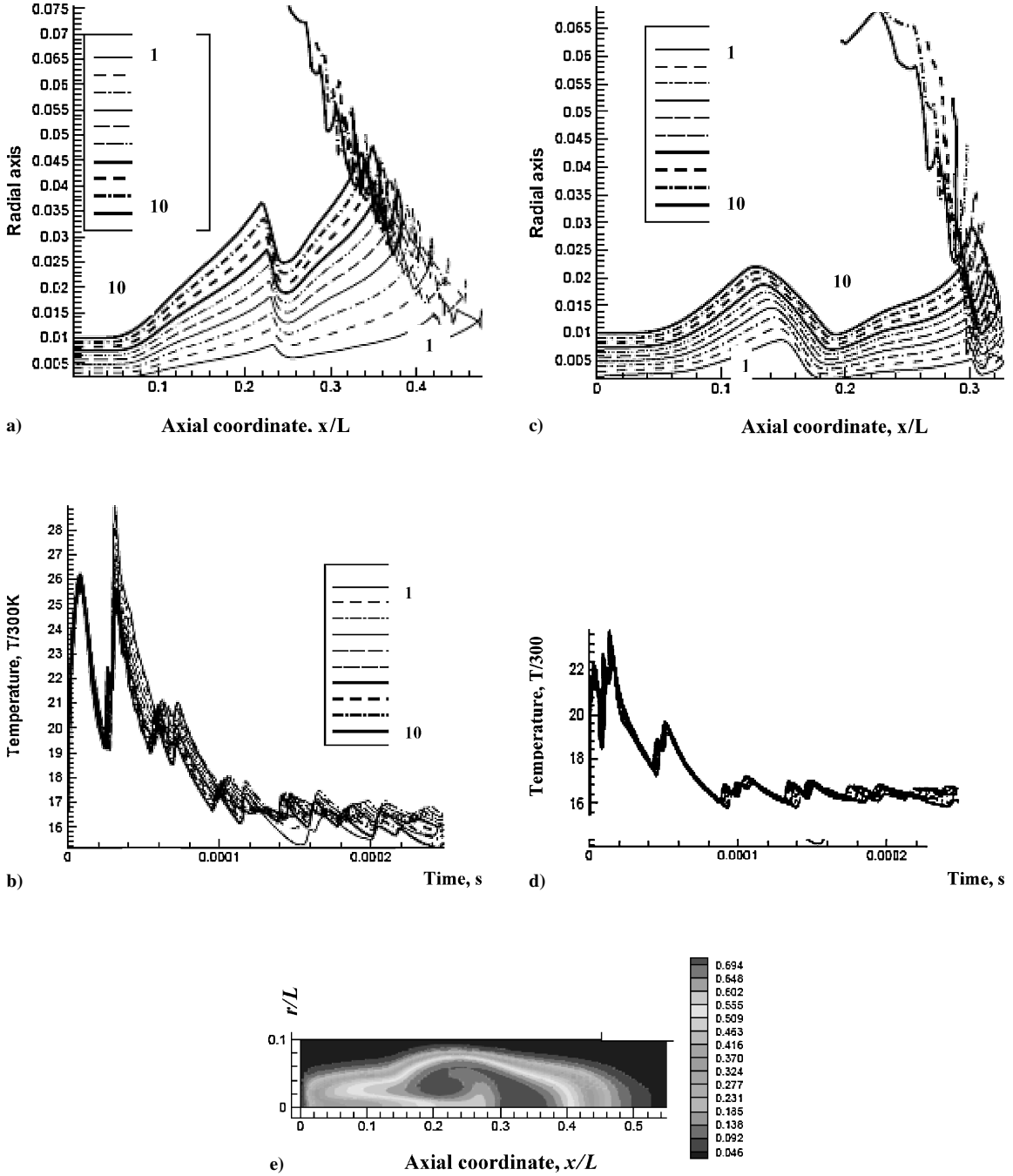

Fig. 13 Long-time dynamics of catalyst particles for doubled-pulse laser: a and b) trajectories and temperature of catalyst particles emerging with the first plume, c and d) trajectories and temperature of catalyst particles emerging with the second plume, and e) concentration (mass fraction) of plume material at $t = 243.0$ μs.

with the plume. The mushroom structure for a merged double plume is considerably larger than that for a single plume. (Compare Figs. 13e and 10a.) High-temperature peaks are avoided, however, and the temperature does not exceed 6600 K during the first 50 μs.

To study the time evolution of the series of 20 plumes, numerical simulations have been conducted under the same initial and boundary conditions as those stated earlier for a single plume under the standard atmospheric pressure of the laser furnace. The time duration between two consequent plumes equals 5.0 μs, whereas

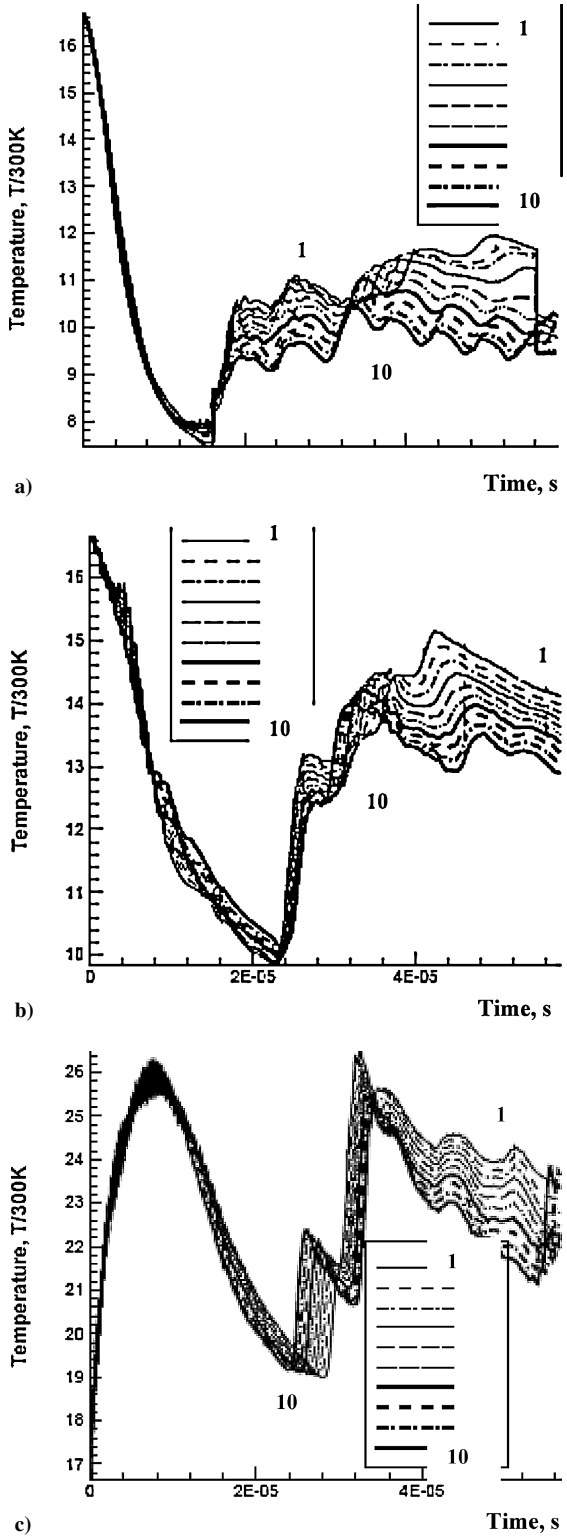

Fig. 14 Temperature of catalyst particles emerging with the 10th plume for various injection speeds: a) $\Omega = 0$, b) $\Omega = 5c_\infty$, and c) $\Omega = 15c_\infty$.

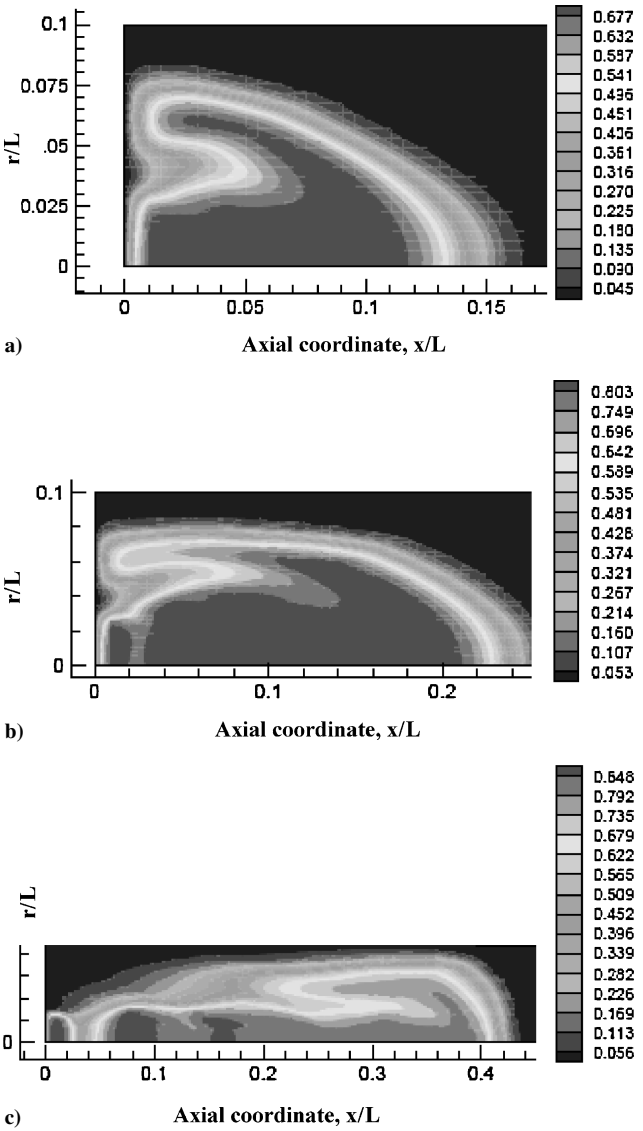

Fig. 15 Concentration of plume material after injection of the 10th plume for various injection speeds: a) $\Omega = 0$, b) $\Omega = 5c_\infty$, and c) $\Omega = 15c_\infty$.

the duration of each single pulse equals 20 ns. The temperature of catalyst particles emerging with the 10th plume is shown in Figs. 14a, 14b, and 14c, when $\Omega = 0$, $5c_\infty$, and $15c_\infty$, respectively. In Figs. 15a, 15b, and 15c, the carbon mass concentration is shown immediately after the emergence of the plume for $\Omega = 0, 5c_\infty$, and $15c_\infty$, respectively.

The temperature of particles has changed substantially compared with the results presented for single and double plumes in the current research. The most striking change is the broad spread of the temperature for various particles. (Compare Figs. 10d and 13c.) The temperature difference between the first particle (emerging near the target center) and the tenth particle (emerging from the periphery of the target) reaches 800 K at $\approx$50 μs. For zero injection velocity, the magnitude of the spread of the catalysts' temperatures is similar to that for the single plume and multiple plumes. (Compare Figs. 9b and 13a.) However, for multiple-plume injection, the temperature spread of catalyst particles starts earlier ($t \approx 20$ μs) than that for the single-plume injection.

In general, the temperature of particles for multiplume injection has increased substantially in comparison with the single- and double-plume cases. The temperature increase is a result of adding of high-enthalpy multiple plumes in the considered physical system. This energy is released in high-temperature domains behind shock waves where the catalyst particles are heated. However, the temperature of catalyst particles may have strong oscillations,

whereas particle cross shock wave fronts originated from different injected plumes and are located close to each other. The heating features of catalyst particles depend on the time interval between injections of the plume, the size of the experimental setup, and the injection velocity.

To investigate repetitiveness of the temperature behavior of catalyst particles for the larger number of plumes, the results for the 20th plume were compared to those for the 10th plume. The temperature of catalyst particles emerging with the 10th and 20th plumes shows identical behavior for the entire range of injection velocities $0 \leq \Omega \leq 15c_\infty$.

VI. Summary

In the LA process, the solid carbon substrate is gasified by the energy of a laser beam and emerges into the ambient gas of the laser furnace. The temperature of catalyst particles emerging with the plume has been obtained as a function of time. The thermal regime of the catalyst particles is crucial to modeling chemical reactions leading to the nucleation of nanotubes. The influence of chamber pressure, injection velocity, and periodicity of the plume on the nonmonotonic temperature behavior of catalyst particles has been investigated.

The presented mathematical model of the plume dynamics in explosive flow is based on Euler equations combined with inviscid equations for the concentration of a gaseous carbon and surrounding inert gas. It has been shown that the influence of viscosity and turbulence on plume dynamics is small for the considered time interval of $\sim$200 μs after plume ablation. The catalysts follow path lines of continuous gas flow. In the complex motion of an ablated plume, the direction of a path line with respect to shock waves and discontinuities is not known a priori. The temperature and kinematics of particles as functions of time are not explicitly observed in the framework of the Eulerian approach. The Lagrangian approach to the motion of the catalyst particles reveals important features of their heating and is adopted in this study.

A relaxing TVD scheme developed for the gasdynamics of a single chemical component appears to be suitable for the modeling of multispecies plume dynamics in LA. Numerical tests have shown that the relaxing TVD scheme is suitable for the numerical simulations involving a high-pressure ratio between the ablated carbon and surrounding gas. Strong shock waves and large gradients of conserved variables are correctly presented by this numerical scheme.

The background pressure in a laser furnace could vary from near-vacuum to atmospheric pressure. Both cases are relevant to existing LA technologies. The reasons for the nonmonotonic behavior of the catalyst particle temperature have been identified as 1) the interaction of the particles with reflected shock waves and 2) a combined radial and axial motion of the catalyst particles through zones of high-temperature gradients caused by the formation of stagnation points and slip lines. Although both reasons are important for a near-atmospheric pressure of the ambient gas, the latter reason plays the key role for a near-vacuum ambient pressure. For plume ablation in low ambient pressure, the blast shock wave and reflected shock waves propagate far ahead of the plume. Consequently, the secondary reflected shock waves are weak when catalysts intersect them. In this case, the nonmonotonic temperature of catalyst particles is caused by the temperature gradients near the slip lines.

For a given average pressure in a laser furnace, the position of the plume depends primarily on the plume injection velocity. The plume injection velocity strongly affects the plume evolution and dynamics of catalyst particles. Existing LA technologies vary widely in terms of laser pulse duration, delivered energy, and the size of the target. These factors strongly affect the injection velocity.The plume propagation speed, the shape of the plume, and its possible backward motion are determined by the interaction of the pressure gradient in the flowfield behind the front blast wave and the density gradient in the plume. The temperature of catalyst particles substantially increases with the increase of injection velocity. For greater injection velocity, the carbon plume propagates faster and is affected more by reflected shock waves that lead to a substantial increase of the amplitude of temperature oscillations.

The modeling of the injection of a series of plumes is important for technological applications such as larger-scale production of carbon nanotubes where a laser hits the target many times. Interactions between two plumes and the dynamics of a multiplume series are addressed in the current study. The temperature of the catalyst particles for injected multiple plumes has been studied, and the reasons for a substantial difference of the temperature profile of the catalyst particles in comparison to a single-plume model have been discussed. The influence of a multiple-plume injection is found to be controversial. On the one hand, the temperature of the catalyst particles for a multiplume injection has increased substantially in comparison to the single- and double-pulse cases. On the other hand, there is a broader spread of temperatures for the catalyst particles emerging from different zones of the target compared to the single-plume case. A refined laser melting and vaporization model of laser–target interaction is needed to determine the injection velocity and time interval between injections of the plume injection and will be addressed in future research.

Acknowledgments

The authors were supported by the Natural Sciences and Engineering Research Council Grant awarded to the second author. For the final part of work, the second author was supported by start-up funds and a Faculty Summer Research Fellowship from the University of Akron. The authors thank the Centre de Recherche en Calcul Applique (Montreal) for their hospitality and computational facilities made available during this research. The first author thanks Ian Stewart, University of Bristol, Bristol, England, United Kingdom, for his comments. The authors acknowledge anonymous reviewers for their suggestions leading to improvement of this paper and the formulation of directions for future research.

References

[1]Yakobson, B., and Smalley, R., "Fullerene Nanotubes: C 1.000.000 and Beyond," *American Scientist*, Vol. 85, 1997, p. 324.

[2]Puretzky, A. A., Schittenhelm, H., Fun, X., Lance, M. J., Allard, L. F., and Geohegan, D. B., "Investigation of Single-Wall Carbon Nanotube Growth by Time-Restricted Laser Vaporization," *Physical Review B: Solid State*, Vol. 65, No. 24, 2002, pp. 245425-1–245425-9.

[3]Greendyke, R., Scott, C., and Swain, J., "CFD Simulation of Laser Ablation in Carbon Nanotube Production," AIAA Paper 2002-3026, June 2002.

[4]Anisimov, S. I., Bauerle, D., and Lukyanchuk, B. B., "Gas Dynamics and Film Profiles in Pulsed-Laser Deposition of Materials," *Physical Review B: Solid State*, Vol. 48, No. 16, 1993, pp. 12,076–12,081.

[5]Mao, S. S., Mao, X., Greif, R., and Russo, R. E., "Influence of Preformed Shock Wave on the Development of Picosecond Laser Ablation Plasma," *Journal of Applied Physics*, Vol. 89, No 7, 2001, pp. 4096–4099.

[6]Chen, K. R., Leboeuf, J. N., Wood, R. F., Geohegan, D. B., Donato, J. M., Liu, C. L., and Puretzky, A. A., "Mechanisms Affecting Kinetic Energies of Laser-Ablated Materials," *Journal of Vacuum Science and Technology*, Vol. A14, No. 3, 1996, pp. 1111–1114.

[7]Arepalli, S., Nikolaev, P., Holmes, W., and Scott, C. D., "Diagnostics of Laser-Produced Plume Under Carbon Nanotube Growth Conditions," *Applied Physics A: Materials Science and Processing*, Vol. 70, No. 2, 2000, pp. 125–133.

[8]Scott, C., Povitsky, A., Dateo, C., Gokcen, T., Willis, P. A., and Smalley, R. E., "Iron Catalyst Chemistry in Modeling a High Pressure Carbon Monoxide Nanotube Reactor," *Journal of Nanoscience and Nanotechnology*, 2003, Vol. 3, No. 2, pp. 63–73.

[9]Povitsky, A., and Salas, M., "Thermal Regime of Catalyst Particles in Reactor for Production of Carbon Nanotubes," *AIAA Journal*, Vol. 41, No. 11, 2003, pp. 2130–2142.

[10]Quirk, J., and Karni, S., "On the Dynamics of Shock-Bubble Interaction," *Journal of Fluid Mechanics*, Vol. 318, 1996, p. 131.

[11]Povitsky, A., and Ofengeim, D., "Numerical Study of Interaction of a Vortical Density Inhomogeneity with Shock and Expansion Waves," *International Journal of Computational Fluid Dynamics*, Vol. 12, 1999, pp. 165–176.

[12]Lobao, D. C., "An Implicit Time Marching Procedure for High-Speed Flow," AIAA Paper 93-3315, July 1993.

[13]Kurganov, A., and Tadmor, E., "New High-Resolution Central Scheme for Conservative Laws of Convection-Diffusion Equations," *Journal of Computatonal Physics*, Vol. 160, No. 1, 2000, pp. 241–282.

[14]Nessyahu, H., and Tadmor, E., "The Convergence Rate for Approximate Solutions for Nonlinear Scalar Conservation Laws," *SIAM Journal of Numerical Analysis*, Vol. 29, No. 6, 1992, pp. 1505–1519.

[15]Strang, G., "On the Construction and Comparison of Difference Schemes," *SIAM Journal of Numerical Analysis*, Vol. 5, No. 3, 1968, pp. 506–517.

[16]Lobao, D., and Povitsky, A., "Furnace Geometry Effects on Plume Dynamics in Laser Ablation," *Mathematics and Computers in Simulation*, Vol. 65, April 2004, pp. 365–383; also *Proceedings of ICCSA-2003*, *Lecture Notes in Computer Science*, Vol. 2668, May 2003, pp. 871–880.

[17]Jin, S., and Xin, Z., "The Relaxation Schemes for Systems of Conservation Laws in Arbitrary Space Dimensions," *Communications on Pure and Applied Mathematics*, Vol. 48, No. 3, 1995, pp. 235–276.

[18]Yee, H. C., "A Class of High-Resolution Explicit and Implicit Shock-Capturing Methods," NASA TM-101088, Feb. 1989.

[19]Yee, H. C., and Harten, A., "Implicit TVD Schemes for Hyperbolic Conservation Laws in Curvilinear Coordinates," AIAA Paper 85-1513, July 1985.

[20]Harten, A., and Lax, P. D., "On a Class of High Resolution Total Variation Stable Finite-Difference Schemes," *SIAM Journal on Numerical Analysis*, Vol. 21, No. 1, 1984, pp. 1–23.

[21]Aregba-Driollet, D., and Natalini, R., "Discrete Kinetic Schemes for Multidimensional Systems of Conservation Laws," *SIAM Journal on Numerical Analysis*, Vol. 37, 2000, pp. 1973–2004.

[22]Zheng, Y., *Systems of Conservation Laws: Two-Dimensional Riemann Problems*, Birkhäuser, Boston, 2001, p. 317.

[23]Banda, M. K., and Seaid, M., "A Class of Relaxation Schemes for Two-Dimensional Euler Systems of Gas Dynamics," *Lecture Notes in Computer Science*, Vol. 2329, April 2002, pp. 930–939.

[24]Sedov, L. I., *Similarity and Dimensional Methods in Mechanics*, Academics Press, New York, 1959.

[25]Zeldovich, Y. B., and Raizer, Y. P., *Physics of Shock Waves and High-Temperature Hydrodynamic Phenomena*, Academic Press, New York, 1966.

[26]Dabora, E. K., "Variable Energy Blast Waves," *AIAA Journal*, Vol. 10, No. 10, 1972, pp. 1384–1386.

[27]Kim, J. U., Clemens, N. T., and Varghese, P. L., "Experimental Study of an Underexpanded Pulsed Laser-Jet," AIAA Paper 99-0452, Jan. 1999.

[28]Kim, K. J., and Wilson, D. E., "Theoretical Analysis of a Plasma Jet Impinging on a Nonreacting Surface," AIAA Paper 99-0455, Jan. 1999.

[29]Bergmann, H. W., "Excimer Laser Induced Surface Modifications and Matter Interaction Using Double-Pulse Technique," *Applied Surface Science*, Vol. 96, April 1996, pp. 287–295.

[30]Knochenmuss, R., and Vertes, A., "Time-Delayed 2-Pulse Studies of MALDI Matrix Ionization Mechanisms," *Journal of Physical Chemistry B*, Vol. 104, No. 23, 2000, pp. 5406–5410.

J. Bellan
Associate Editor